Scaling to the MERIS Resolution: Mapping Accuracy and Spatial Variability

Freek van der Meer*, Wim Bakker, Klaas Scholte and **Andrew Skidmore**
International Institute for Aerospace Survey and Earth Sciences (ITC),
Division of Geological Survey, P.O. Box 6,7500 AA Enschede, the Netherlands

Steven de Jong and **Michiel Dorresteijn**
University of Utrecht, Department of Physical Geography,
P.O. Box 80115, 3508 TC Utrecht, the Netherlands

Jan Clevers and **Gerrit Epema**
Wageningen University and Research Centre, Centre for Geoinformation,
P.O. Box 339, 3700 AH Wageningen, The Netherlands

Abstract

Within the framework of ESA's Earth Observation Program, the Medium Resolution Imaging Spectrometer (MERIS) is developed as one of the payload components of the ENVISAT-1. MERIS is a fully programmable imaging spectrometer, however a standard 15 channel band set will be transmitted for each 300 m. pixel (over land) covering the visible and near-infrared wavelength range. Since MERIS is a multidisciplinary sensor providing data that can be input into ecosystem models at various scales, we studied MERIS performance relative to the scale of observation using simulated data sets degraded to various resolutions in the range of 12m. to 300m. Algorithms to simulate MERIS data using airborne imaging spectrometer data sets are presented, including a case study from GERIS 63 channel data over a agricultural site in central Spain (the Almaden test site). Through a pixel purity analysis, end members are derived from the MERIS-type data and subsequently used as input to a spectral unmixing analysis yielding fraction of end member (abundance) images. The original data as well as the abundance images are spatially analyzed using variogram surfaces and mapping accuracy is modeled at various spatial scales. We observe differences between the sampling resolutions (i.e., pixel size) found to be optimal for the different ground cover types. I he optimal scale for observing different components of spectral mixtures varies depending on the type of mixture, however, the best possible resolutions in all cases of mixtures studied is below the envisaged 300 m. field of view for the MERIS sensor. The analysis of semivariogram surfaces demonstrates that the spatial distribution of the variance of the mixtures is invariant with scale, thus the observed mapping discrepancies are not related to the data processing but to the observations themselves.

Introduction

The use of spatial statistics embedded in regionalized variables theory for the analysis of remotely sensed data dates back to the pioneering work of P.J. Curran and C.E. Woodcock in the late 1980's. Contemporaneously these authors explored the use of the semivariogram, i.e., a curve showing variance versus sample spacing, to describe patterns in remotely sensed imagery (Woodcock *et al*. 1988a+b; Curran 1988). Since that time, many new applications of geostatistics to aid in image interpretation and enhancement have been developed including: replacement of missing or bad data values (Atkinson *et al*. 1990; Rossi *et al*. 1994), estimating signal to noise (Curran & Dungan 1989), noise removal (Green *et al*. 1988), estimating measurement error (Atkinson 1997), mapping (Dungan *et al*. 1994), classification (Van der Meer 1994) and the use of co-kriging to combine field and image data (Atkinson *et al*. 1994; Van der Meer 1998). A recent summary of results can be found in Stein *et al*. (1998). With the advent of new spaceborne sensors with variable and selectable spatial and spectral resolution the factor of scale and selection of optimal support size in remote sensing becomes a pressing issue. Research in this field dates back to 1987 (Woodcock & Strahler 1987) and has recently been revived (Atkinson & Curran 1995). Related to this, issues of up-and downscaling are common problems combining geostatistical practice and remote sensing (see Stewart *et al*. 1998 for a

* Presently at: Delft University of Technology, Faculty of Civil Engineering & Geosciences, Department of Technical Earth Sciences, Mijnbouwstraat120, 2600 GA Delft, The Netherlands

Geocarto International, Vol. 15, No. 1, March 2000
Published by Geocarto International Centre, G.P.O. Box 4122, Hong Kong.

recent review.

Within the framework of ESA's Earth Observation Programme, the Medium Resolution Imaging Spectrometer (MERIS) is developed as one of the payload components of the ENVISAT-1, proposed for launch on the first European Polar Platform scheduled for 1999 (Rest *et al.* 1991; Bézy *et al.* 1996). MERIS (Rest *et al.* 1999) is an advanced optical sensor with high spectral and moderate spatial resolution designed to acquire remote sensing data of relevance to environmental management and to the understanding of up- and downscaling from regional to global scales. The MERIS optical arrangement is set up in such a way that six contiguous optical modules view the earth through a deflecting mirror, thus subdividing the 1150 km total field of view into six slightly overlapping sub-scenes (each module covering approximately 14º; Rast *et al.* 1991, Morel *et al.* 1993). The MERIS main performance requirements are shown in table 1. Table 2 shows the 15 channels that will be transmitted as the MERIS standard band set. MERIS is designed as a multidisciplinary mission aimed at oceanographic applications as well as at atmospheric and vegetation features. The sensor should provide data that can be input into ecosystem models that are used for environmental modeling. Since the optimal scale of measuring related variables may be dependent on the type and nature of the parameter of study, it is important to evaluate MER1S' potential relative to the scale of observation. In this paper we present simulated MERIS data derived from airborne imaging spectrometer data sets and derive products useful for land applications at various spatial resolutions. These products are used to assess the mapping accuracy of the variable and indicate the relative optimal spatial resolution to be achieved. This leads to a better understanding of the expected performance of the sensor for different land applications.

Simulating Data from ESA's Medium Resolution Imaging Spectrometer

Image (or spectral) simulation is only possible when the source sensor has a spatial and spectral resolution finer and better respectively than the target simulated sensor (Justice *et al.*, 1989). The Spectral Resampling of existing airborne/ spaceborne data sets towards the MERIS spectral properties are not described in detail in the literature. Investigators mention a simulation of MERIS data (Doerffer *et al.*, 1995; Verstraete *et al.*, 1995), however without details on resampling procedures of the existing wavebands and centres towards the MERIS specifications. Spatial resampling

Table 1 MERIS main performance requirements based on Cutter *et al.* (1989), Rast *et al.* (1991), Rast & Bézy (1995) and the MERIS web site http://www.estec.esa.nl/envisat/Satellite/Instruments/MERIS/.

MERIS	Specification	Cutter *et al.* (1989)	Rast *et al.* (1991)	Rast and Bézy (1995)	web site
SYSTEM					level IB-
				Product	
	Liftime			4 years	
	Data rate: Reduced Resolution Mode (RR)		1.5Mbits/s	1.6Mbits/s	
	Full Resolution Mode FR)		22.5Mbits/s	24.0 Mbits/2	
GEOMETRIC					
	Instrument Field of View (IFOV)	82º	81.52º	68.5º centred about nadir	68.5º
	Swath width Envisat-1 orbit	1500 km	1450km	1150	1150
	Spatial Resolution: RR		1200	1200	1200
	FR	260 m	250	300	300
	Locialisation Accuracy without use of Landmarks			<2 km	
SPECTRAL	Spectral range	400-1050 nm	400-1050 nm	390-1040 nm	400-1050 nm
	Spectral Sampling Interval	1.25 nm-40 nm	1.25 nm	1.25 nm	1.25m
	Transmitted/Programmable Bands	30	15	15	15
	Spectral Band width		10 nm; 685-=5 nm	1.25 -30 nm	2.5-20nm
	Registration Between Bands			0.12 RR IFOV	
	Band Centre knowledge			< 1nm	
RADIO-	Polarisation Sensitivity	<1%	<1%	<0.4 over full spectral range	
METRIC	Radiometric Accuracy	400-1000<2% relative to sun		390-900<2% relative to sun	400-900 < 2%
					900-1050<5%
	Dynamic Range	albedo=1		up to albedo=1	
	S/N (over open ocean)		778 (b2); 190 (b8); 54 (15)	from 1500 (b1) to 200 (b14)	
OTHER	Depointing Angle	app. 20º along track			
	Orbit Envisat-1		sun synchronous polar	sun synchronous polar	
	Inclination		98.5º	98.5º	
	Nodal Crossing Time (descending)		9:55 AM	10:00AM	
	Mean Orbital Altitude		800 km	800km	

methods are described by Justice *et al.* (1989) and Teillet and Staenz (1992). Both use a spatial filter (gaussian blur filter) and sampling mechanism (Fast Fourier Transforms) to simulate coarse resolution data. Some simulation studies have been conducted to aid in the understanding of other future spaceborn imaging spectrometers including MODIS (Kaufman el al. 1997) and ASTER (Abrams & Hook, 1995) again without documenting details on processing strategies. We followed a essentially two-step procedure

A. Spectral resampling
   - convolution over sensors Spectral Response Function for each band in case of oversampled input data
   - band matching in case of undersampled input data

B. Spatial resampling
   - spatial degradation using the sensor's Point Spread Function for each band The procedures are described in detail below.

Spectral resampling

As a general rule in simulation it can be stated that only spectrally oversampled image data cubes can be used to generate channels of future sensor data types. We have explored the use of AVIRIS, CASI, DAIS 7915 and GERIS 63 channel imaging spectrometer data (Figure 1) to simulate MERIS. The GERIS 63 channel airborne imaging spectrometer system and the DAIS 79 channel imaging spectrometer system do not allow to simulate MERIS channels by means of spectral gaussian re-sampling. For these systems, only band matching techniques can be applied in which the best matching bands are selected to represent the designated MERIS channels. In case of NASA's Airborne Visible/ lnfrared Imaging Spectrometer (AVIRIS) and Compact Airborne Spectrographic Imager (CASI) over-sampling the MERIS channels allows the use of gaussian re-sampling. This procedure involves estimating the gaussian spectral response function (SRF) of each MERIS channel using the band center and width (in full-width-half-maximum). This SRF is of the type

$$R_i(\lambda_i) = \frac{1}{\sigma\sqrt{2\pi}} e^{-0.5(\lambda-\mu)^2/\sigma^2} \qquad [1]$$

where μ is the band centre, σ the standard deviation (equivalent to the FWHM) of the channel and λ the wavelength relative to μ and $R_i(\lambda)$ the spectral response. Note that the integral over the SRF of Y is 1. For each MERIS channel the spectral response curve is calculated using the gaussian approximation of Eq. 1. The channels of the higher spectral resolution airborne imaging spectrometer data set that are within the wavelength range of the selected MERIS channel are integrated by dividing them into the derived SRF assuming that the initial SRF of the input data channels are a single bright source (i.e., a continuous input spectrum). This is done as follows

$$\rho_{res}(\lambda_i) = \frac{\int_{\lambda_1}^{\lambda_2} \rho(\lambda) R_i(\lambda) d\lambda}{\int_{\lambda_1}^{\lambda_2} R_i(\lambda) d\lambda} \qquad [2]$$

Table 2 The MERIS 15 spectral bands. Note that the 765 rim channel as described in former publications (Doerffer *et al.* 1995; Bezy *et al,* 1996) is excluded (pers. comm. Mike Rast? 1998).

Band Nr	Band centre (nm)	Band width (nm)	Potential Applications
1	412 5	10	Yellow substance, Turbidity
2	442 5	10	Chlorophyll absorption maximum
3	490	10	Chlorophyll, other pigments, polarisation measurement
4	51 ()	I ()	Turbidity Suspended sediment, Red tides
5	560	10	Chlorophyll reference, Suspended sediment
6	620	10	Suspended sediment
7	665	10	Chlorophyll absorption
8	681.25	7.5	Chlorophyll fluorescence
9	705	10	Atmospheric correction, Red Edge
10	753.75	7.5	Oxygen absorption reference
11	760	2.5	Oxygen absorption R-branch
12	775	15	Aerosols, vegetation
13	| 65	20	Aerosols corrections over ocean
14	| 90	10	Water Vapour Absorption Reference
15	900	10	Water Vapour Absorption

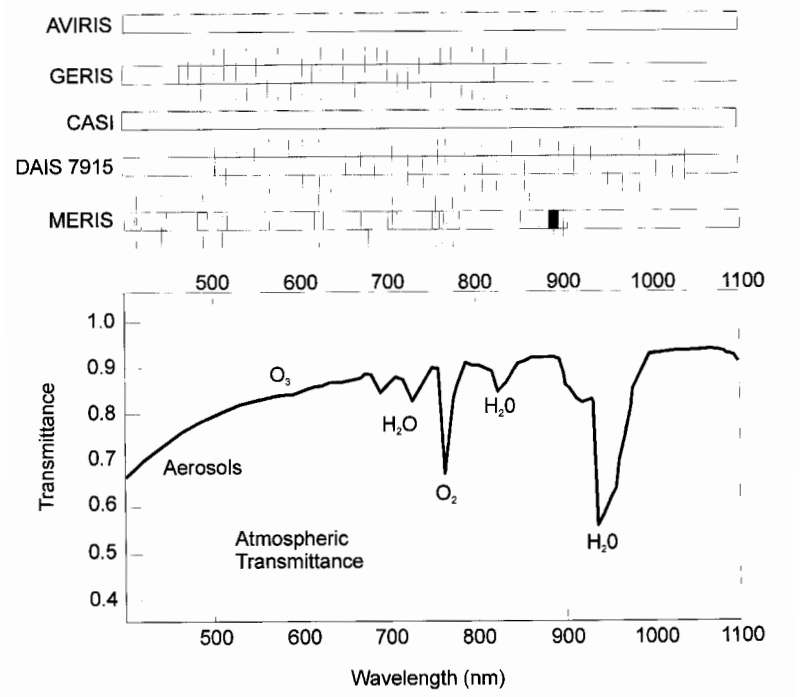

Figure 1 Atmosphere spectrum with main gas absorption bands indicated. The topmost par of' the figure shows the wavelength coverage (bar) and the channels center wavelengths (vertical lines) for MERIS and four airborne imaging spectrometer systems which can be used to simulate MERIS data.

where $\rho_{res}(\lambda_i)$ is the re-sampled spectrum using the continuous spectrum $\rho(\lambda)$ and the SRF $R_i(\lambda)$. This deconvolution is achieved by integrating between the lower (λ_1) and upper(λ_2) wavelength limit of the designated (i.e., to be simulated) image channel. Since the gaussian SR function only asymptotically approaches zero, we truncated the SRF at 1.5 times the FWHM.

Spatial resampling

Spatial degradation is essentially a two-step process. The first step requires modeling the transfer function between the initial data and the desired data and deriving a spatial filter that allows simulation of the coarse resolution imagery. The second step involves re-sampling to the desired pixel size. As is the case in spectral resampling with the spectral response function, the sensor's Point Spread Function (PSF) gives the spatial responsivity of the sensor. The PSF is defined as (Schowengerdt, 1997)

$$e_b(x,y) = \int_{\alpha_{min}}^{\alpha_{max}} \int_{\beta_{min}}^{\beta_{max}} s_b(\alpha, \beta)\, PSF\,(x-\alpha, y-\beta)\, d\alpha d\beta \qquad [3]$$

where $e_b(x,y)$ is the resulting electronic signal for band b at location given by coordinate (x,y), $s_b(\alpha, \beta)$ is the input signal, whereas the limits of the integral determine the spatial extend in two dimensions, α and β, over which the physical signal is weighted. A common model for the PSF like the spectral integration of Eq. 1 is given by

$$PSF\,(x, y) = \frac{1}{2\pi ab} e^{-x^2/2a^2 e^{-y^2/2b^2}} \qquad [4]$$

where a and b determine the width of the optics of the PSF in the cross- and along track direction. In the absence of details on the PSF for MERIS, we used a normalized detector PSF which is equivalent to applying a square moving average filter of the desired spatial resolution

$$PSF\,(x, y) = \frac{1}{ab} \sum_{a=1}^{a} \sum_{b=1}^{b} s_b \qquad [5]$$

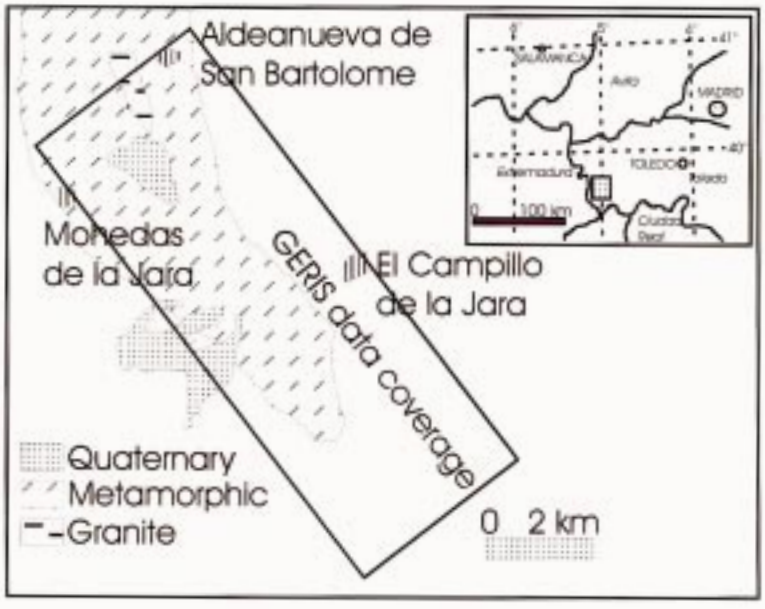

Figure 2 Location of the study area and GERIS data take.

MERIS image products

As a preliminary analysis of scale effects in MERIS data simulation we used atmospherically corrected GERIS 63 channel imaging spectrometer data from the Almaden study site (see Figure 2 for location and Figure 3 for a sample image) in Central Spain acquired during the EISAC '89 campaign and generated a 15 band MERIS sample data set at various spatial resolutions between the original 12m. resolution and the 300m. MERIS resolution. The Almaden study site is an agricultural test site with typical large scale patches of farm land which was mostly bare during time of acquisition. The area is underlain by two granitic intrusions of leucocratic type. Details on the area and image pre-processing can be found in Fan *et al*. (1997). From the atmospherically corrected GERIS data the channels matching the MERIS bands were extracted following

Figure 3 Color composite image of GERIS bands 35, 26, and 4 displayed in RGB with decorrelation stretching applied.

Table 3. This resulted in a MERIS data cube at the original 12 m. GERIS resolution. This cube was subsequently re-sampled stepwise from 12 m. Up to approximately 300 m. following the degradation process described earlier. The process is illustrated in Figure 4. In order to derive ground abundances of various Earth materials we applied spectral unmixing to the data cube.

We used the 12m. resolution "MERIS" data set to find the purest endmember pixels. We used the Minimum Noise Fraction (MNF) transformation of Green *et al*. (1988) to determine the spectral dimensionality defining the number of end members needed to optimally describe the spectral variability. The MNF transformation is a two-step principal component transformation where during the first step using the noise covariance matrix the noise is decorrelated to have unit variance and no band-to-band correlation. The second principal component transformation results in a data set where components are ranked in terms of noise equivalent radiance. Consider stochastic variables $\mathbf{Z(x)} = [Z_1(\mathbf{x})...Z_p(\mathbf{x})]^T$ with expectation $E\{\mathbf{Z}\} = 0$ and dispersion $\mathbf{D}\{\mathbf{Z}\} = \Sigma$. New mutually orthogonal variables with maximum signal-to-noise ratio can be constructed as

$$Y_i = a_{i1}Z_1+...a_{ip}Z_p=a_i^T Z, i=1,....,p \qquad [6]$$

Assuming additive noise (i.e., $\mathbf{Z(x)} = \mathbf{S(x)} + \mathbf{N(x)}$ where **S** and **N** are uncorrelated signal and noise components, respectively) the response equals $\Sigma = \Sigma_S + \Sigma_N$ where Σ_S and Σ_N are dispersion matrices for **S** and **N**, respectively. The signal-to-noise ratio (estimated from the ratio of mean and variance in a local window) for Y_i that needs to be maximised can be defined as (Lee *et al*. 1990; Nielsen and Larsen, 1994)

$$\frac{VAR\{a_i^T\mathbf{S}\}}{VAR\{a_i^T\mathbf{N}\}} = \frac{a_i^T \Sigma a_i}{a_i^T \Sigma_N a_i} - 1 = \frac{1}{\lambda_i} - 1 \text{ and } \frac{a_i^T \Sigma_N a_i}{a_i^T \Sigma a_i} = \lambda_i \qquad [7]$$

the factors λ_i are the eigenvalues of Σ_N with respect to Σ and the factors a_i are the corresponding conjugate eigenvectors. The inherent spectral dimensionality of the data set can be found by examining the eigenvalues and associated MNF images. Some of these MNF images are associated with large eigenvalues and coherent (MNF) eigenimages while the remainder if the MNF bands have near-unity eigenvalues and images dominated by noise. Thus the MNF eigenvalues and eigenimages yield the absolute number of end-members required to model the image spectral response. The locations of the end member pixels in the image data are found using the Pixel Purity Index (PPI; Boardman *et al*. 1995). The PPI is based on the approach developed by Smith *et al*. (1985). This approach regards spectra as points in an *n*-dimensional space (*n* being the number of bands). The body (referred to as simplex) that spans the data points in a *n*=2-dimensional space is a triangle having *n*+1 facets. The purest end-members are found at the locations in this space where the sides of the triangle intersect. This principle can be extended to higher dimensions in a similar way. The PPI approach compares the pixels in a scene with the best fitting simplex and records the number of times a pixel is found at the extreme facets of the simplex. Portraying this as an image

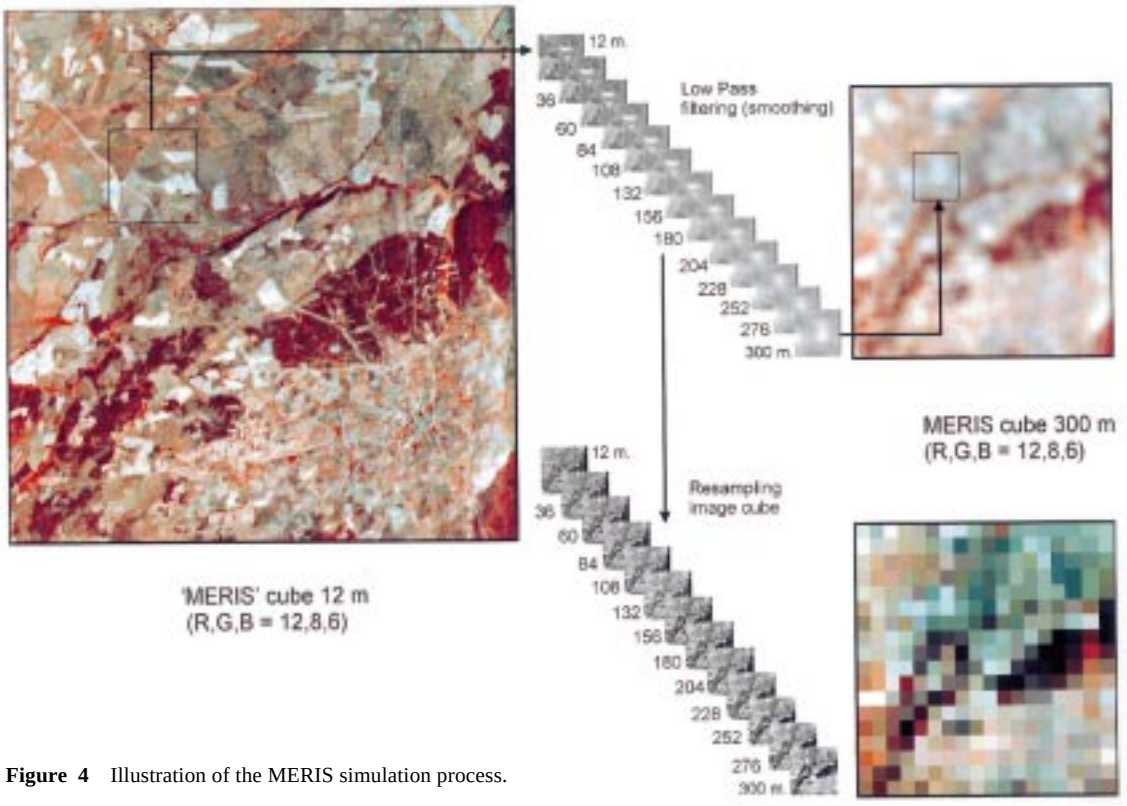

Figure 4 Illustration of the MERIS simulation process.

Table 3 Some airborne imaging spectrometers and the available bands to simulate MERIS spectral bands using the principle of direct band matching.

MERIS		GERIS		DAIS		CASI			AVIRIS		
No.	Wavelength	No.	Wavelength	No.	Wavelength	No.	No.	Wavelength	band no	No.	Wavelength
1	0.4125	-		-		4 tm 10	7	0.4121	5,6	5	0.41175
2	0.4425	-		-		22 tm 27	24	0.4417	8,9	8	0.4408
3	0.49	2	0.489	1	0.501	49 tm 54	52	0.4907	13,14	13	0.48967
4	0.51	4	0.514	2	0.517	60 tm 66	63	0.5101	15,16	15	0.50934
5	0.56	8	0.564	5	0.567	88 tm 94	91	0.5595	20,21	20	0.55874
6	0.62	13	0.625	8	0.621	122 tm 128	125	0.6198	26,27	26	0.61824
7	0.665	16	0.662	11	0.671	148 tm 153	150	0.6644	30,31	31	0.66779
8	0.68125	18	0.687	12	0.689	157 tm 162	159	0.6805	34,35	35	0.68491
9	0.705	19	0.699	13	0.705	170 tm 175	173	0.7055	37,38	37	0.70398
10	0.75375	23	0.794	16	0.756	198 tm 202	200	0.7539	42,43	42	0.75174
11	0.76	24	0.761	16		203,204	203	0.7593	43	43	0.7613
12	0.775	25	0.774	17	0.773	208 tm 216	212	0.7755	44,45	44	0.77086
13	0.865	-		22	0.86	256 tm 267	262	0.8653	53,54,55	54	0.86665
14	0.89	-		24	0.895	273 tm 278	276	0.8905	56,57	56	0.88583
15	0.9	-		24		279 tm 284	281	0.8995	57,58	57	0.89542

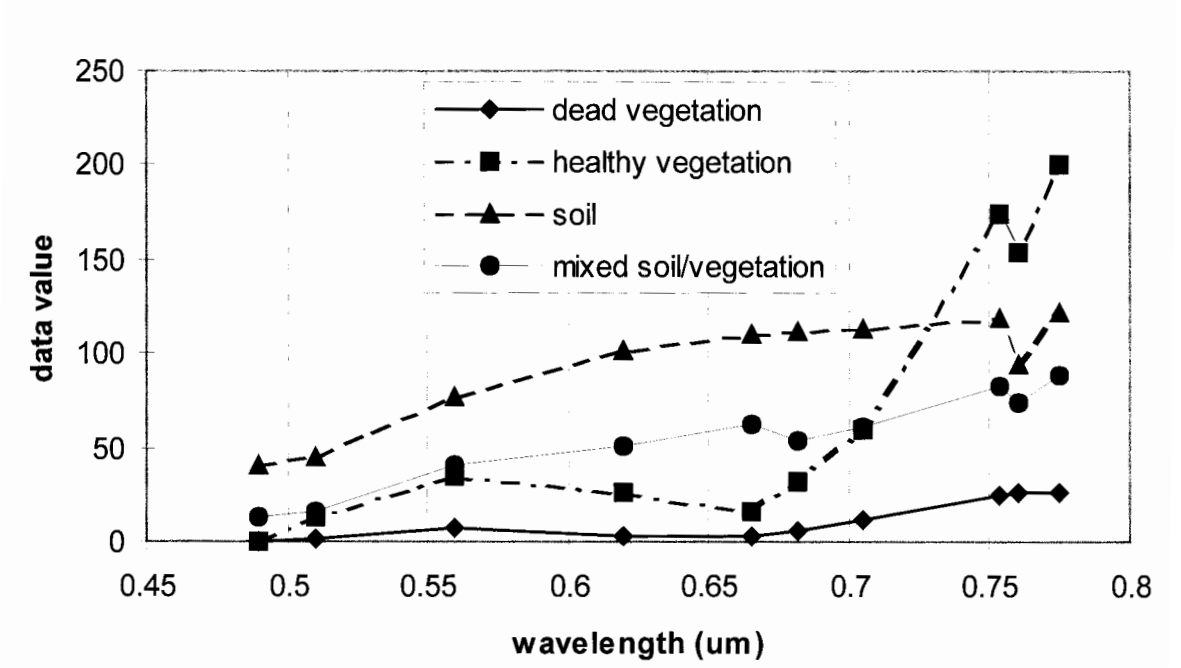

Figure 5 MERIS-type end members derived through pixel purity index.

of cumulative count values allows identification of the locations in the data space of the initial set of spectrally pure end members. The resulting end member spectra were used as input to a spectral unmixing analysis to gain surface fractional abundance estimates of various ground cover types. Examples of some of the MERIS end members derived are shown in Figure 5. The unconstrained spectral unmixing technique we used is further described in Settle & Drake (1993). These authors define a vector of expected pixel signals $\mu_i = \{\mu_{i1}, \mu_{i2} ..... \mu_{in}\}^T$ for the n ground cover classes giving an expected mixed pixel signal under strictly linear conditions as

$$f_1\mu_1 + f_2\mu_2....f_c\mu_c = Mf \qquad [8]$$

The columns of the matrix M are the vectors μ_i which are the end-member spectra. The observed signal of pure pixels will exhibit statistical fluctuations due to sensor noise characterized by a noise variance-covariance matrix N_i. Therefore pixels with the mixture f will exhibit fluctuations around their mean value Mf characterized by the noise covariance matrix N(f) given by

$$N(f) = f_1 N_1 + f_2 N_2....+ f_c N_c \qquad [9]$$

If the N(f) is independent of f, thus when the noise components are un-correlated, the linear model can be defined according to Settle & Drake (1993) as

$$x = Mf + e \qquad [10]$$

where e is the vector of errors satisfying

$$E(e) = 0 \text{ and } E(ee^T) = N \qquad [11]$$

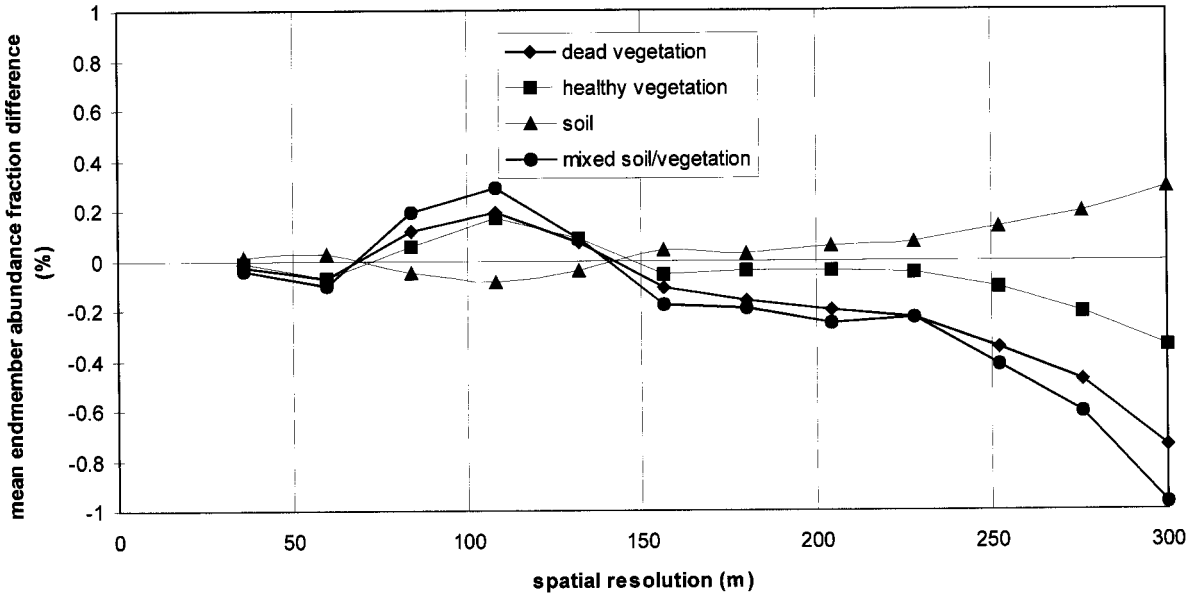

Figure 6 Mean difference of the abundance estimated at coarse resolution as compared to the highest possible resolution of 12 m.

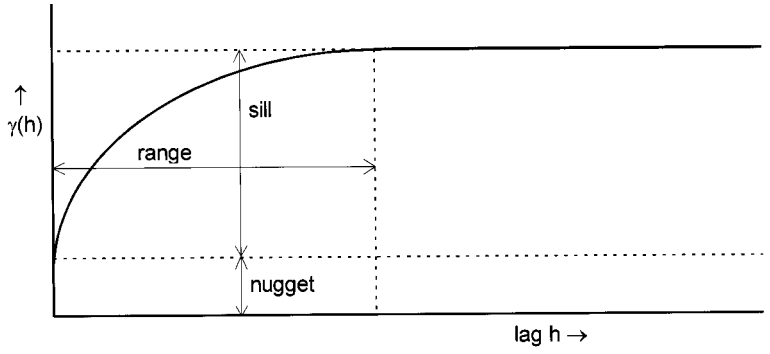

Figure 7 Illustration of a variogram model curve and indication of key parameters describing the model.

This signifies that the expectation of e is zero and that the expectation of noise component is close to the sensor noise component. The final result were end member abundance images for several end members of which we focus our analysis on the "vegetation" and "soil" end member. A first result derived from these end member abundance estimates is shown in Figure 6 where we have calculated the mean difference in the fraction for the different scales (i.e., pixel sizes) as compared to the 12 m. resolution results. From Figure 6 we can observe an inflection point in the behavior of the trends in abundances at 100 m. resolution. By means of geostatistical techniques, we will further analyze the spatial variability in the end member fraction images at the various spatial resolutions to better understand the observed discrepancy illustrated in Figure 6.

Spatial variability

Regionalized variable theory assumes that spatial variation of a variable z can be expressed as the sum of three components

$$z(x) = m(x) + e'(x) + e'' \qquad [12]$$

where x is the position, $m(x)$ is the structural component (a trend or a mean), $\varepsilon'(x)$ is the term denoting the stochastic, spatially dependent residuals from $m(x)$, and ε'' is a residual, spatially uncorrelated (Gaussian) noise. Once structural effects have been accounted for, the remaining variation is homogeneous in its variation, so that differences between samples should merely be a function of the distance between them. This spatial relationship can be expressed by a variogram (or semivariogram), which is a graph of semivariance versus sample spacing. The variogram in remote sensing can be estimated from p(h) pairs of observations, $z_v(x_l)$ and $z_v(x_l+h)$ with 1=1,2,...,p(h) as

$$\gamma(h) = 1/2\, p(h) \sum_{l=1}^{p(h)} \{z_v(x_l) - z_v(x_l + h)\}^2 \qquad [13]$$

Parameters of a fitted mathematical junction (the variogram model) may include a range, a nugget and a sill. The range of the variogram indicates a spatial scale of the pattern, the nugget is an indication of the level of uncorrelated noise in the data and the sill reveals the total variation (Figure 7). The resulting variograms for two directions corresponding to maximum and minimum variability are shown in Figure 8. Variograms of remotely sensed measurements should be interpreted with care. In remote sensing, the support size (the area or volume of the samples) equals the sample spacing. i.e. reflection values are averaged over the pixel size of the measuring device. Furthermore, the sensor's output is always a derivative of the complex composition of radiation from the terrain. Some major points for variogram interpretation are (De Jong & Burrough 1995; Figure 7)

- The range is related to sizes of objects in the terrain (for example batches of shrubs);

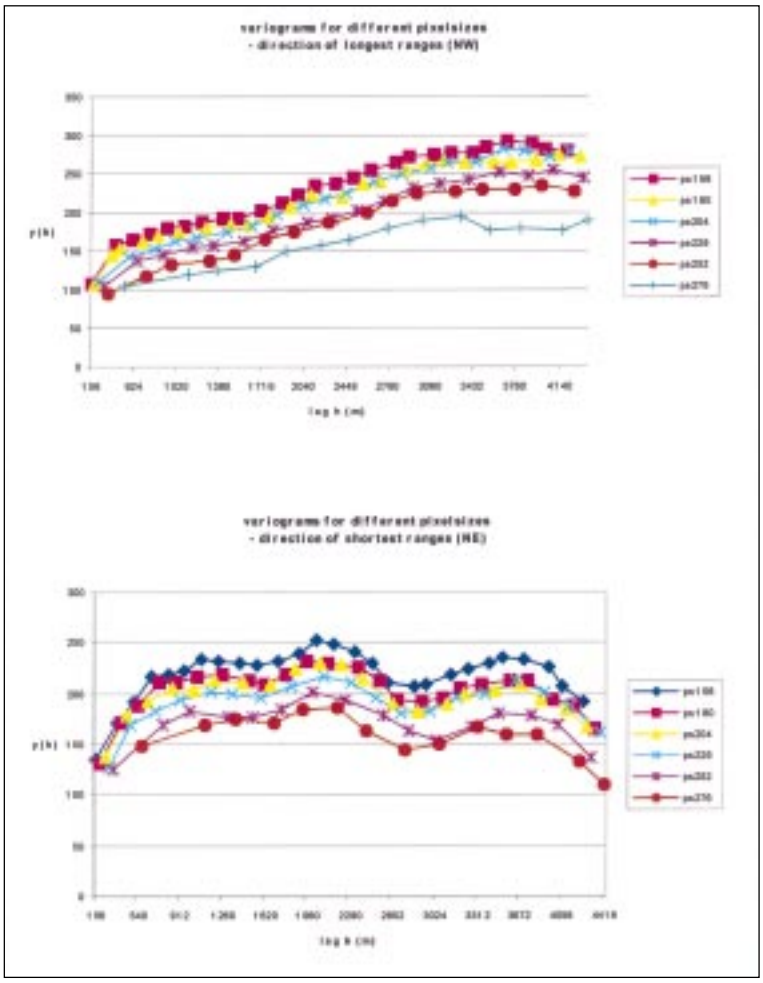

Figure 8 Directional variograms in northwest (top) and northeast (bottom) direction for pixel sizes ranging from 156 up to 276 m.

- The shape of the variogram is related to variability in size of objects in the terrain;
- The height of the variogram is influenced by the density of coverage of the objects and the spatial differences between the objects;
- Regularisation (coarsening the spatial resolution) reduces the overall variance of the data and blurs fine scale variation; consequently, the sill height will reduce, the range will increase and the nugget will increase;
- Anisotropy in the image is expressed by the variation of variogram parameters with the direction of the transect.

An effective way to detect and display anisotropies in the pattern occurring variability is a variogram surface. In this surface the (semi)variance is not only related to the mere distance between two points (the lag), but also to the direction. In calculating the variogram value for pairs of points separated by a vector (h_x, h_y) all pairs are grouped together whose separation is $h_x \pm \Delta x$, $h_y \pm \Delta y$. In this case Δx and Δy are half the support size, i.e. (in a rectangular coordinate system) the pixelsize (Isaaks & Srivastava, 1989). The result is a surface with for each vector a computed (semi)variance.

Variogram surfaces for simulated MERIS band 7 (Figure 9) were analyzed showing a strong directional anisotropy and little change in spatial structure with change in pixel size. Figure 10 shows two

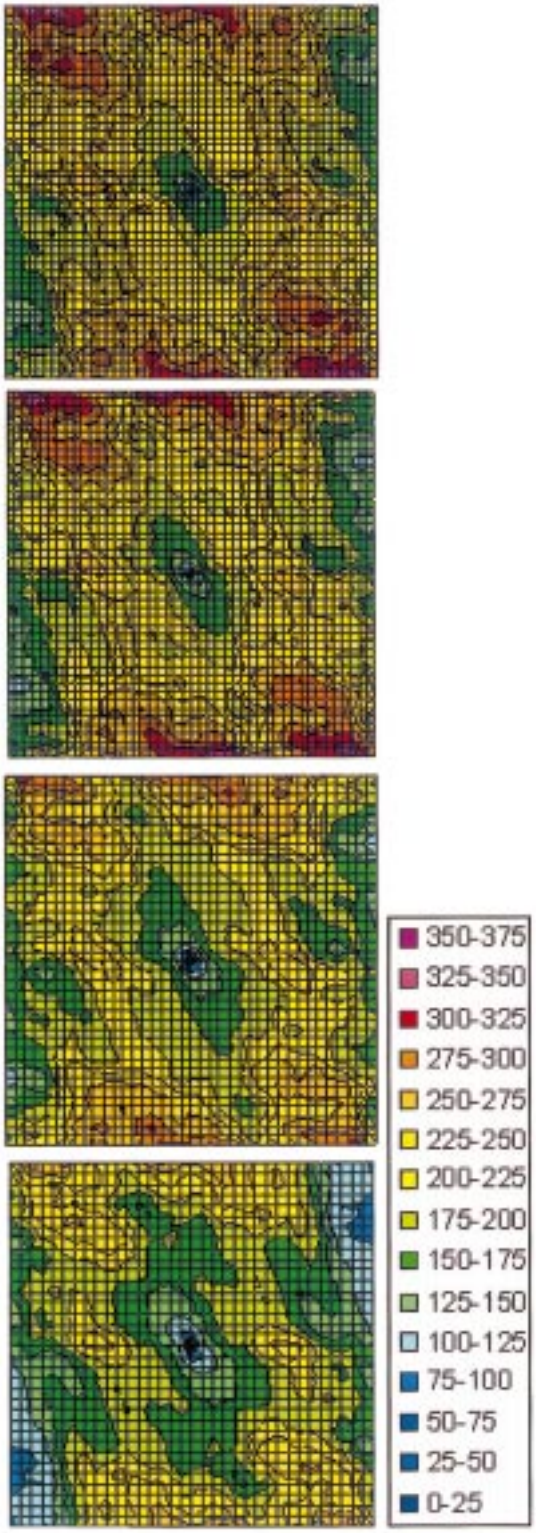

Figure 9 Variogram surfaces at (from top to bottom) 180, 204, 228 and 252 m. resolution for MERIS band 7 showing strong anisotropy.

variogram surfaces for the end member abundance images for "soil" and "vegetation" at 300 m. resolution again showing surprisingly little change in spatial structure between these end members.

Mapping accuracy: optimal sampling sizes.

Woodcock & Strahler (1987) developed a method for selecting a optimal spatial resolution in terms of the spatial variation of an image. Let $z(x_{ij})$ be the value of the pixel located at x_{ij} in the ith row and the jth column of a image. The local variance can be computed over a (2n+1) x (2m+1) w indow by

$$\sigma_{ij}^2 = 1/(2n+1)(2m+1) \sum_{k+i-nl=j-m}^{i+n \; j+m} \Sigma \{z(x_{kl})-u_{ij}\}^2 \qquad [14]$$

where u_{ij} is the mean of the (2n+1) x (2m+1) window centered on x_{ij}. The local variance can be computed for varying pixel sizes using degraded image products. A plot of local variance versus pixel size allows selection of the optimal pixel size corresponding to the peak in variability (Figure 11). For the "soil" end member a decrease of local variance with spatial resolution is found thus indicating that the optimal sampling size is equal to the highest possible resolution. For the "vegetation" end member a peak is found at around 100 meter resolution. Thus not only do we observe difference between the sampling resolutions (i.e., pixel size) found to be optimal for different ground cover types, but they also both are smaller than the resolution to be imaged by MERIS (i.e., 300 m.). Another observation made is that the optimal scale for observing different components of spectral mixtures varies depending on the type of mixture. Again, the best possible resolutions in all cases is below the envisaged 300 m. field of view.

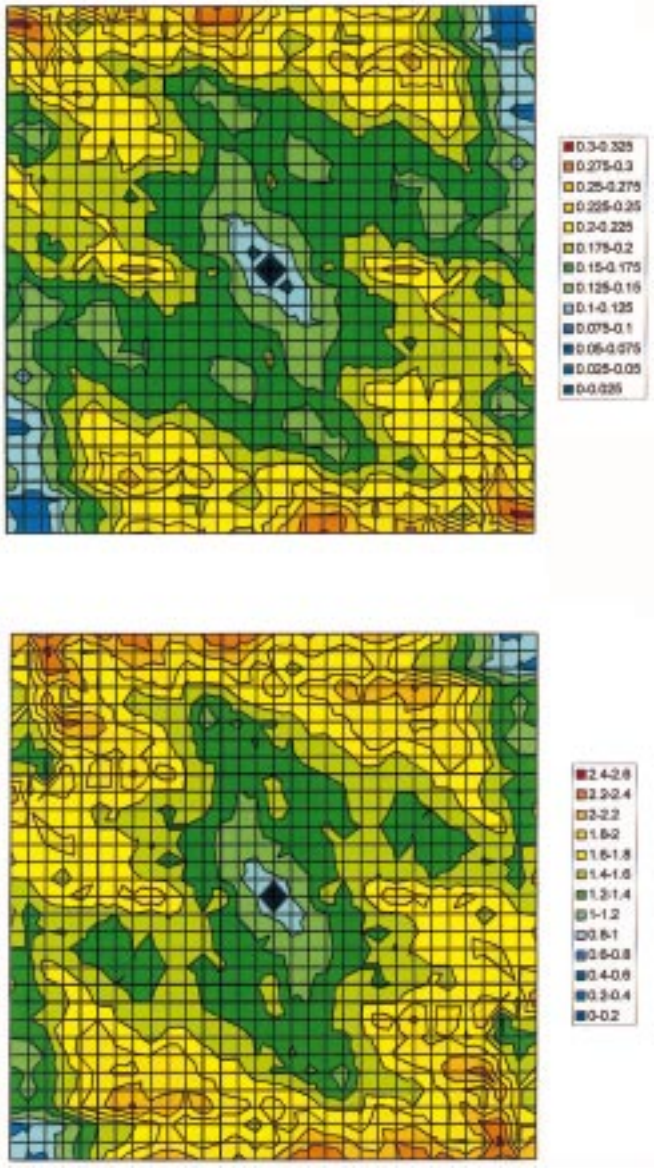

Figure 10 Variogram surfaces for the "soil" end member (top) and the "vegetation" end member (bottom) at the MERIS resolution of 300 m.

Conclusions

Given the limitations of currently available airborne imaging spectrometer systems it has been shown that MERIS data can be simulated. In order to evaluate the spatial aspects of this data, variograms and variogram surfaces are calculated for MERIS band 7 and fractional abundance estimates for a "soil" and a "vegetation" endmember. These allow to gain insight into the nature of the data and its spatial dependency showing however little noticeable changes even at a sub-pixel level. However when evaluating mapping accuracy clearly different optimal sampling sizes are found for the different end members. For both endmembers, the optimal sampling size corresponding to the peak in the local variance curve is found at finer resolution than the pixel size proposed for MERIS. We observe differences between the sampling resolutions (i.e., pixel size) found to be optimal for different ground cover types. The optimal scale for observing different components of spectral mixtures varies depending on the type of mixture, however, the best possible resolutions in all cases of mixtures studied is below the envisaged 300 m. Held of view for the MERIS sensor. The analysis of semivariogram surfaces clearly shows that the spatial distribution of the variance of the mixtures is invariant with scale, thus the observed mapping discrepancies are not related to the data processing but to the observations themselves.

Acknowledgment

This research is conducted as part of the MERILand project (http://www.itc/nl/~MERIS/) partially funded by the Netherlands Remote Sensing Board (BCRS) under contract 3.1/AP-06. Advice by Mike Rast and Steve Delwart (ESA-ESTEC) and Ingrid Janssen (BCRS) was highly appreciated.

References

Abrams, M. & Hook, S.J. 1995. Simulated ASTER data for geologic studies. IEEE Transaction on Geoscience and Remote Sensing 33: 692-699.

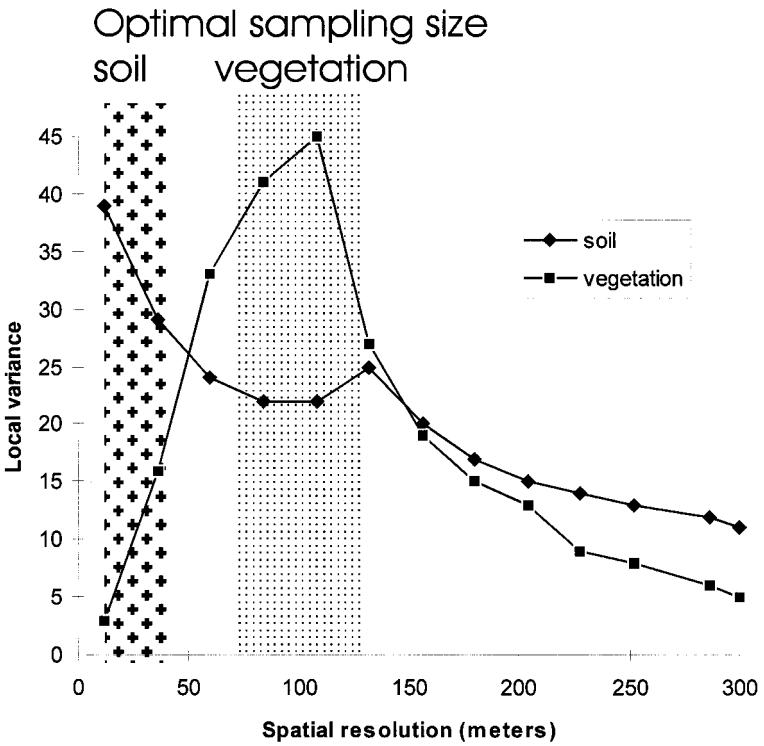

Figure 11 Plot of local variance versus pixel size. The peak of this curve corresponds to the optimal sampling ground resolution (pixel size) for imaging the designated class.

Atkinson, P.M. & Curran, P.J. 1995. Optimal size of support for remote sensing investigations: defining an optimal sampling strategy. IEEE Transaction on Geoscience and Remote Sensing 33: 768776.

Atkinson, P.M., Curran, P.J. & Webster, R. 1990. Sampling remotely sensed imagery for storage, retrieval and reconstruction. Professional Geography 37: 345-353.

Atkinson, P.M., Webster, R. & Curran, P.J. 1994. Cokriging with airborne MSS imagery. Remote Sensing of Environment 50: 335-345.

Atkinson, P.M. 1997. On estimating measurement error in remotely-sensed images with the variogram. International Journal of Remote Sensing 18: 3075-3084.

Bézy, J.L., M. Rast, S. Delwart, P. Merheim-Kealy & S. Bruzzi 1996. The ESA Medium Resolution Imaging Spectrometer (MERIS). Backscatter 7:14-19.

Boardman, J.W., Kruse, MA. & Green, R.O. 1995. Mapping target signatures via partial unmixing of AVIRIS data. In: *Proceedings of the Fifth JPL Airborne Earth Science Workshop*, JPL, Publication 951, Vol.1, pp. 23-26.

Curran, P.J. 1988. The semivariogram in remote sensing: an introduction. Remote Sensing of Environment 24: 493-507.

Curran, P.J. & Dungan, J.L. 1989. Estimation of signal-to-noise: a new procedure applied to AVIRIS data. IEEE, Transaction on Geoscience and Remote Sensing 27: 630-628.

Cutter, M.A., D.R. Lobb, Y. Ramon, G. Ratier and J. Bézy (1989). A Medium Resolution Imaging Spectrometer for the European Polar Orbiting Platform. In: *Advanced Optical Instrumentation for Remote Sensing of the Earth's Surface from Space (SPIE)*, Vol. 1129, pp.l07-116.

De Jong, S.M. & Burrough, P.A. 1995. A fractal approach to the coossification of Mediterranean vegetation types in remotely sensed images. Photogrammetric Engineering and Remote Sensing 61: 1041-1053.

Doerffer, R., K.Sörensen and J. Aiken (1995). MERIS: Potential for Coastal Zone Application. In: P . J. Curran & Y. C . Robertson (eds.), *Proceedings of the 21st Annual Conference of the Remote Sensing Society (RSS 95), "Remote Sensing in Action"*, 11-14 September, University of Southampton, pp. 166-175.

Dungan, J.L., Peterson, D.L. & Curran, P.J. 1994. Alternative approaches for mapping vegetation quantities using ground and image data. In. W. Michener, S. Stafford & J. Brunt (eds.). *Environmental information management and analysis: ecosystem to global scales*. Taylor & Francis. London, pp. 237261.

Fan, L., van der Meer, F. & Bodechtel, J. 1997. Geological information extraction from airborne hyperspectral data and field spectral data in a heavily soil and vegetation covered area. In: *Proceedings of the Third International Airborne Remote Sensing Conference and Exhibition*, 7-10 July 1997, Copenhagen, Denmark, Vol. I, pp. 665-672.

Green, A.A., Berman, M., Switzer, P. & Graig, M.D. 1988. A transformation for ordering multispectral data in terms of image quality with implications for noise removal. IEEE Transactions on Geoscience and Remote Sensing 26: 65-74.

Isaaks, H.S. & Srivastava, R.M. 1989. *Applied Geostatistics. Oxford University Press*, New York. Oxford, 561 pp.

Justice, C.O., Markham, B.L., Townshend, J.R.G. & Kennard, R.L. 1989. Spatial degradation of satellite data. International Journal of Remote Sensing 10: 1539- 1561.

Kaufman, Y.J., A.E. Wald, L.A. Remer, B.C. Gao, R.R. Li & L. Flynn 1997. The MODIS 2.1-μm channel-correlation with visible reflectance for use in remote sensing of aerosol. IEEE Transactions on Geoscience and Remote *Sensing 35: 1286-1298.*

Lee, J.B., Woodhyatt, S., and Berman, M., 1990, Enhancement of high spectral resolution remote-sensing data by a noise-adjusted principal components transform. IEEE Transactions on (geoscience and Remote Sensing, **28**, 295-304.

Morel, M., J.L. Bézy, F. Montagner, A. Morel & Fischer, J. 1993. Envisat's Medium-Resolution Imaging Spectrometer: MERIS. ESA Bulletin 76: 40-46.

Nielsen, A.A., and Larsen, R., 1994, Restoration of GERIS data using the Maximum Noise Fractions Transform. In *Proceedings of the First International Airborne Remote Sensing (conference and Exhibition (ERIM)*, Strassbourg, France (Ann Arbor: ERIM International), pp. 557-568.

Rast, M. & Bezy, J.L. 1995. The ESA Medium Resolution Imaging Spectrometer (MERIS): Requirements to its Mission and Performance of its System. In: P.J. Curran & Y.C. Robertson (eds.), *Proceedings of The 21St Annual Conference of the Remote Sensing Society (RSS 95), "Remote Sensing in Action"*, 11-14 September, University of Southampton, pp.l25-132.

Rast, M., Bézy, J.L. & Bruzzi, S. 1999. The ESA Medium Resolution Imaging Spectrometer MERIS — a review of the instrument and its mission. International Journal of Remote Sensing, 20(9): 1681 1702.

Rast, M., Bézy, J.L., Morel, M. & Fanton d'Andon, O. 1991. The performance of the ESA Medium Resolution Imaging Spectrometer (MERIS). In: *Physical Measurements and Signatures in Remote Sensing Proceedings of the 5th International Colloquium* (ESA SP-319, May, 1991), pp. 147-152.

Rossi, R.E., Dungan, J.L. & Beck, L.R. 1994. Kriging in the shadows: geostatistical interpolation for remote sensing. Remote Sensing of Environment, 49: 32-40.

Schowengerdt, R.A., 1997. Remote Sensing — models and methods for image processing (second edition). Academic Press, Boston: 522 pp.

Settle, J.J. & Drake, N.A. 1993. Linear mixing and the estimation of ground cover proportions. International Journal of Remote Sensing 14, 1159-1177 (1993).

Smith, M.O., Johnston, P.E. & Adams, J.B. 1985. Quantitative determination of mineral types and abundances from reflectance spectra using principal component analysis. Journal of {geophysical Research 90: 797-804.

Stein, A., Bastiaanssen, W.G.M., de Bruin, S., Cracknell, A.P., Curran, P.J., Fabbri, A.G., Gorte, B.G.H., van Groenigen, J.W., van der Meer, F. & Saldaña, A. 1998. Integrating spatial statistics and remote sensing. International Journal of Remote Sensing, 19: 1793-1814.

Stewart, J.B., Engman, E.T., Feddes, R.A. & Kerr, Y.H. 1998. Scaling up in hydrology using remote sensing: summary of a workshop. International Journal of Remote Sensing, 19: 181194.

Teillet, S. & Staenz, K. 1992. Atmospheric Effects Due to Topography on MODIS Vegetation Index Data Simulated From AVIRIS Imagery over Mountainous Terrain. Canadian Journal of Remote Sensing 18: 443-441.

Van der Meer, F. 1994. Extraction of mineral absorption features from high-spectral resolution data using non-parametric geostatistical techniques. International Journal of Remote Sensing, 15: 2293-2214.

Van der Meer, F. 1998. Mapping dolomitization through a co-regionalization of simulated field and image-derived reflectance spectra; a proof-of-concept study. International Journal of Remote Sensing' 19(8): 1615-1620.

Verstraete, M.M., B. Pinty and P.J. Curran 1995. MERIS Potential for Land Applications. In: P.J. Curran & Y.C. Robertson (eds.), *Proceedings of the 21St Annual Conference of the Remote Sensing Society (RSS 95), "Remote Sensing in Action"*, 11-14 September, University of Southampton, pp. 15716.

Woodcock, C.E. & Strahler, A.H. 1987. The factor of scale in remote sensing. Remote Sensing of Environment 21: 311 -332.

Woodcock, C.E., Strahler, A.H. & Jupp, D.L.B. 1988a. The use of variograms in remote sensing I. Scene models and simulated images. Remote Sensing of Environment 25: 323-348.

Woodcock, C.E., Strahler, A.H. & Jupp, D.L.B. 1988b. The use of variograms in remote sensing 11. Real digital images. Remote Sensing of Environment 25: 349-379.

Fourteenth International Conference and Workshops

Applied Geologic Remote Sensing

INTEGRATED SOLUTIONS FOR REAL WORLD PROBLEMS

Las Vegas, Nevada 6-8 November 2000

Call for Papers

You are invited to attend the **Fourteenth International Conference and Workshops on Applied Geologic Remote Sensing** to be held 6-8 November 2000 in Las Vegas, Nevada. This international conference primarily focuses on geologic remote sensing and geographic information systems (GIS) with special emphasis on mineral and hydrocarbon exploration, and environmental and engineering applications. The conference will take place at the Alexis Park Hotel, located just east of the world-famous Las Vegas Strip.

With more than 300 technical presentations by experts from more than 30 countries, the program will address all aspects of applied geologic remote sensing, from fundamental principles and techniques to advanced data processing and geologic interpretation. The hands-on workshops, technical tours, and exhibits program of cutting-edge products and services will benefit all users of remote sensing data: large and small, expert or novice. The conference is organized by Veridian ERIM International, in cooperation with National Aeronautics and Space Administration (NASA), U.S. Department of Energy Nevada Operations Office, U.S. Geological Survey, and other leaders in the geologic remote sensing community.

Interested contributors should submit a 250-word summary by **13 March 2000.** Include the conference topic addressed. Notification of your paper's acceptance and an author's kit will be mailed in **May 2000**. Final camera-ready copy will be due by **4 August 2000**.

Accepted summaries received electronically can be accessed on the World Wide Web before and after the conference.

Electronic submissions:
E-mail: geology@erim-int.com
Website: www.erim-int.com/CONF/GRS.html

Written and faxed summaries:
V-ERIM/Geologic Conference
P.O. Box 134008
Ann Arbor, MI 48113-4008 USA
Fax: 1-734-994-5123

Conference Topics

- Mineral Exploration
- Petroleum Exploration/Detection of Hydrocarbons
- Geological Hazards/Disaster Management
- Hydrogeology/Hydrology Mapping
  - Geologic
  - Stratigraphy
  - Soils
  - DEMs
- Operations Support/Engineering
  - Well Sites
  - Pipelines
- GIS Applications
- Environmental Applications
- Archaeological Applications
- Case Histories
- Application of New Data Sources, Sensors, and Measurement Techniques
  - New Satellite Data (e.g., Landsat 7, ASTER)
  - Hyperspectral Sensors
  - Polarimetric Applications
  - Thermal Imagery
  - Lidar
  - Commercial Sources
- Data Access, Integration, and Dissemination
  - Data Fusion
  - Integrated Data Products
  - Digital File Format Standards
  - Internet Delivery of Data

Inquiries Only:
Telephone: 1-734-994-1200, ext. 3234
wallman@erim-int.com

Please provide your complete mail/delivery/e-mail address and facsimile number on all correspondence.

99-20225